Analysis Note: $\psi' \to \pi^+\pi^- J/\psi$, $J/\psi \to l^+l^-$ and $B(J/\psi \to l^+l^-)$

F. A. Harris[1] and Wang Meng[2]

[1]University of Hawaii, Honolulu, HI 96822
[2]Inst. of High Energy Physics, Beijing 100039, China

April 10, 1998

Introduction

The $\psi' \to \pi^+\pi^- J/\psi$, $J/\psi \to l^+l^-$ sample is extremely important. As mentioned previously [1], it is used to determine the line shape of the J/ψ peak in the m_{recoil} distribution in the determination of the number of ψ' events. More importantly, this sample can be used to determine the J/ψ leptonic branching ratios, as well as to study the physics of the $\psi' \to \pi^+\pi^- J/\psi$ process. The branching ratio $B(J/\psi \to ll) \simeq 6.0$ %.

This analysis note describes event selection, background checks, agreement with the Monte Carlo, and the determination of $B(J/\psi \to l^+l^-)$. The study of the physics of the $\psi' \to \pi^+\pi^- J/\psi$ process is covered in a separate note.

Lepton ID

In order to select clean $\psi' \to \pi^+\pi^- J/\psi$, $J/\psi \to l^+l^-$ events, it is necessary to require PID for the leptons, as well as to make kinematic cuts. In the following, we use the new dE/dx and TOF routines of Li Xinhua and Bill Dunwoodie[2].

Fig. 1 shows Xse of one track versus Xse of the other track. Xse is the corrected Xs value assuming the electron hypothesis. We get nice separation of ee events from other events using ONLY dE/dx information, so we will make use of both the drift chamber and the shower counter to identify electrons. This is very useful because Sober does not model the rib region of the shower counter well and gives an underestimate of the electron identification efficiency. In addition, having two independent systems allows us to make comparisons between them to determine the efficiency and background of each. We can use data to determine the PID efficiency!

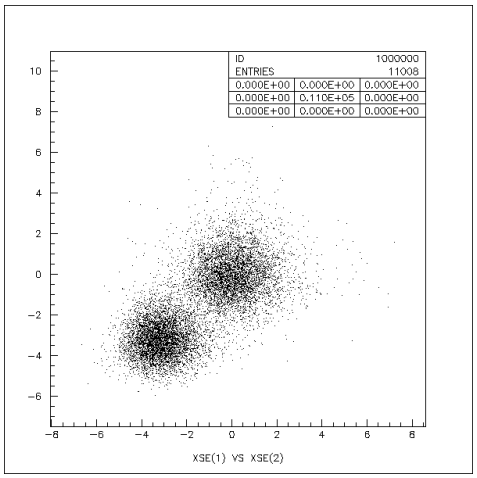

Figure 1: Xse of track 1 versus Xse of track 2, where Xse is calculated assuming that tracks are electrons. Events are $\pi^+\pi^-\mu^+\mu^-$ and $\pi^+\pi^-e^+e^-$ events from the '95 data. The round cluster at (0,0) is due to the e^+e^- events, while the cluster at approximately (-3,-3) is due to the $\mu\mu$ events.

Momentum Dependence of PID

Figs. 2A and 2B show the energy deposited in the shower counter (E) versus momentum (p) for tracks not in the rib region. Electron and muon events are well separated at high momentum. Figs. 2C and 2D show E/p versus p for the same tracks. Again electron and muon events are well separated at high momentum. The separation is poorer at lower momentum. Muon events are flat in E versus p, while electron events are flat in E/p versus p.

Fig. 3 shows Xse versus the momentum. In Fig. 3A, there are clear kaon, proton, and pion bands. Fig. 3B shows where electrons and muons occur on the plot. Clearly there are regions in momentum where protons and electrons overlap and where kaons and electrons overlap in Xse.

ee Selection

We use the following algorithm:

- Define the rib region of the shower counter: $|zsh| < 0.04$m or $0.8 < |zsh| < 1.0$m.
- If both tracks are outside of the rib region and have momenta > 0.8 GeV/c, use the shower counter to define electrons and cut on E/p of track 1 versus E/p of track 2.
- Otherwise, use the drift chamber and cut on Xse of track 1 versus Xse of track 2. Also require $E/p > 0.5$ if one of the tracks is outside the rib region.

The cut is made on z at the shower counter rather than $\cos\theta$ because the resolution is better. The $\cos\theta$ distribution is smeared out because of the z extent of the interaction region.

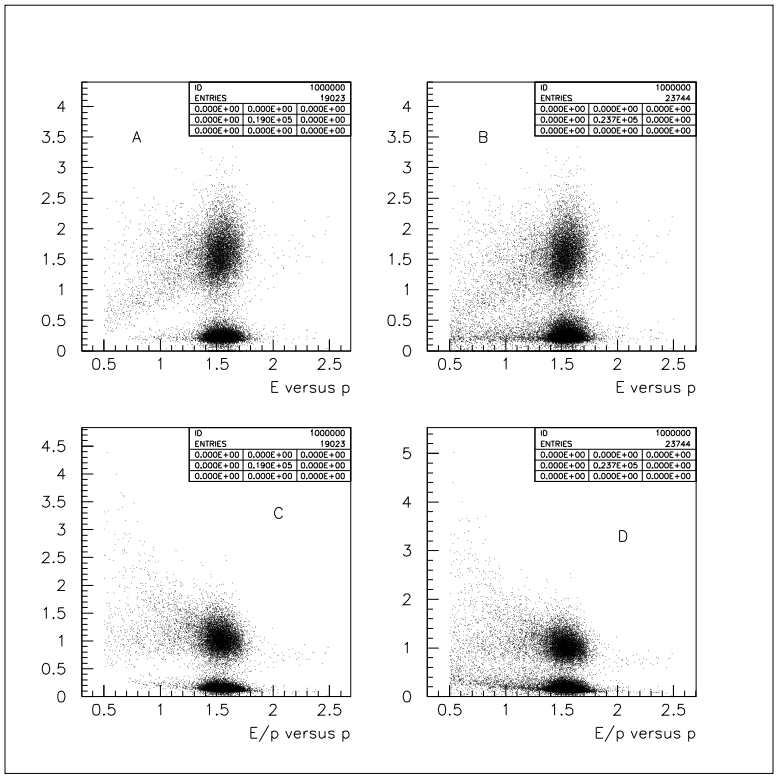

Figure 2: Shower counter energy (E) response versus momentum (p) for $\pi^+\pi^- l^+ l^-$ events using '95 data. A.) E versus p for events with identified leptons; B.) E versus p for events without lepton identification required; C.) E/p versus p with identified leptons; D.) E/p versus p for events without lepton identification required . Most tracks occur at 1.5 GeV/c. The separation at high momentum is very good; it is less so at low momentum.

Figure 3: Xse versus p for $\pi\pi l^+ l^-$ events from the '95 data. A.) Events without identified electrons or muons. Bands due to π's, K's, and protons are clearly visible. B.) Electron and muon events. The upper cluster contains the electron events. Note that electron events overlap proton events at about 1.2 GeV/c and K's at about 0.5 GeV/c.

ee PID Efficiency and Background

Since we have good separation of electrons from other particles in both the drift chamber and the shower counter, we can determine the electron identification efficiency and the background by comparing one system with the other. In Fig. 4, the distribution of E/p of one track versus the E/p of the other is shown for events selected on the basis of Xse of one track versus the Xse of the other for events with neither track in the rib region and with $p > 0.8$ GeV for the '95 data. Most events occur in a cluster centered at (1,1), but there are a few background events located near the origin. By counting the number of background events at the origin, it is possible to determine the Xse vs. Xse cut background rate. By determining how many events in the cluster at (1,1) pass the E/p versus E/p cut, we can determine the efficiency (ϵ_{EP}) of this cut.

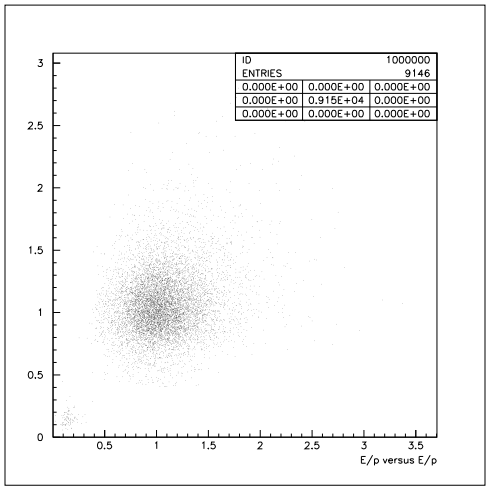

Figure 4: Distribution of E/p for track 1 versus E/p of track 2 for $\pi^+\pi^-e^+e^-$ events outside of the rib region and selected using cuts on Xse of track 1 versus Xse of track 2 for the '95 data. Events near the origin are used to calculate the background associated with the Xse versus Xse cut. Determining how many events in the cluster at (1,1) are inside the E/p versus E/p cut region gives the efficiency of this cut (ϵ_{EP}).

Fig. 5 shows the Xse of one track versus the Xse of the other for events selected on the basis of the E/p versus E/p cut for events with neither track in the rib region in the '95 data. Only a few events occur in the non-electron region (compare this figure with Fig. 1). These are used to determine the background rate associated with the E/p versus E/p cut (ϵ_{Xse}). Determining how many of the electron cluster events pass the Xse versus Xse cut determines the efficiency of this cut.

For events with neither track in a rib region and with both tracks having $p > 0.8$ GeV, ee events are identified using the shower counter with the E/p cuts:

1. $(E/p)_1 > (E/p)_{1cut}$ and $(E/p)_2 > 1$ –OR–
2. $(E/p)_2 > (E/p)_{2cut}$ and $(E/p)_1 > 1$ –OR–

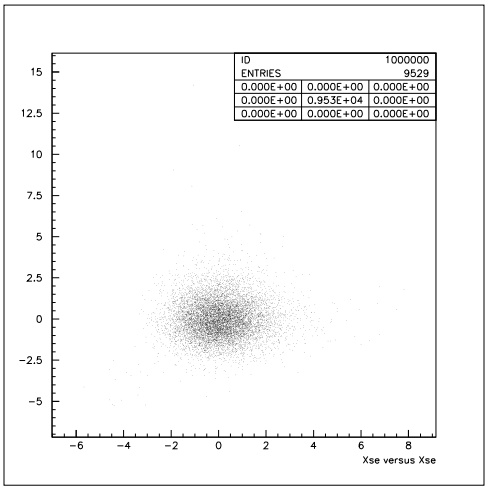

Figure 5: Distribution of Xse for track 1 versus Xse of track 2 for $\pi^+\pi^-e^+e^-$ events outside of the rib region and selected using cuts on E/p of track 1 versus E/p of track 2. Events below the origin and to the left are used to calculate the background associated with the E/p versus E/p cut. Determining how many events are inside the Xse versus Xse cut region gives the efficiency of this cut (ϵ_{Xse}).

3. $(E/p)_r = \sqrt{[(E/p)_1 - 1]^2 + [(E/p)_2 - 1]^2}$ is inside an ellipse formed using $(E/p)_{1cut}$ and $(E/p)_{2cut}$.

The $(E/p)_{cut}$ value depends on p and is given by $(E/p)_{cut} = 0.6/p$.

A complication arises because the E/p distribution of simulated events looks rather different than the E/p distribution of real events. To insure that the correct efficiency is determined when cutting on Monte Carlo events, we shift and scale the Monte Carlo E/p distribution using shifts and scale factors determined by Program MnFit [3]. Fig. 6 shows the E/p distributions for '93 data, for Monte Carlo data, and for shifted and scaled Monte Carlo data.

For events with a track in the rib region or with $p < 0.8$ Gev/c, ee events are identified using the drift chamber with the following cuts:

1. $\sqrt{\frac{Xse(1)^2}{\sigma(1)^2} + \frac{Xse(2)^2}{\sigma(2)^2}} < 2.0$ –OR–

2. If $Xse(1) > 1.0$ or $Xse(2) > 1.0$, $\sqrt{\frac{Xse(1)^2}{\sigma(1)^2} + \frac{Xse(2)^2}{\sigma(2)^2}} < 3.0$.

3. If one track is not in the ribs, E/p of that track must be > 0.5.

For the Xse versus Xse cut, a routine similar to OKXSPI[4] is used. For each data set ('93, '95, 93' Monte Carlo, and 95' Monte Carlo), the mean and two sigmas of a bifurcated Gaussian are determined. All cuts are made in terms of the sigmas (plus side or minus side) for that distribution. This is necessary since the Monte Carlo does not simulate the data well.

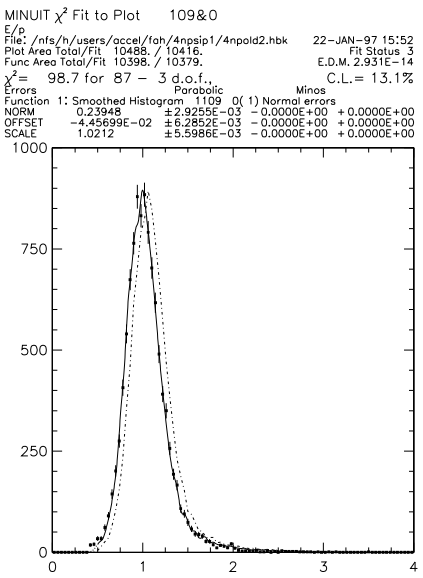

Figure 6: E/p distributions for '93 data (points with error bars), Monte Carlo data (dash-dot curve), and shifted and scaled Monte Carlo data (solid curve). The latter shows good agreement with the '93 data.

Efficiency and Background Results using the final selection cuts plus some additional cuts (see below) are shown in Table 1 for the '93 data and Table 2 for the '95 data. Fig. 7 shows the z distribution of the electron events. The distribution is quite smooth through the rib regions.

Table 1: Efficiencies and Backgrounds of ee Identification Schemes for '93 Data for the final cuts. Overall is determined by weighting according to the percentage of events obtained with the two selection methods.

Method	Background (%)	Efficiency (%)	MC Eff (%)
E/p vs E/p	0.0	98.3	98.7
Xse vs Xse	0.3	94.1	93.6
Overall	0.1	97.1	97.3

Table 2: Efficiencies and Backgrounds of ee Identification Schemes for '95 Data for the final cuts. Overall is determined by weighting according to the percentage of events obtained with the two selection methods.

Method	Background (%)	Efficiency (%)	MC Eff (%)
E/p vs E/p	0.0	96.8	98.4
Xse vs Xse	0.34	95.0	93.4
Overall	0.1	96.3	97.0

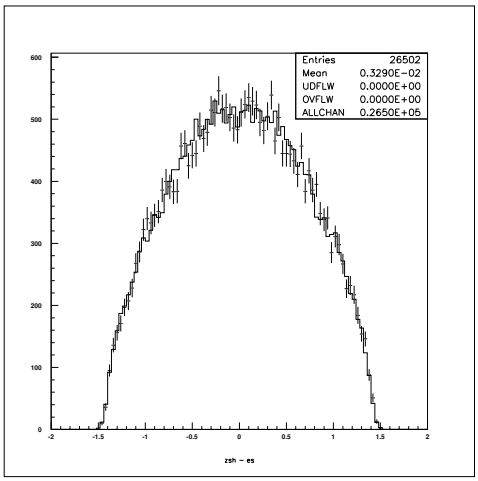

Figure 7: Distribution of the z coordinate at the shower counter for identified electron in $\psi' \to \pi^+\pi^- J/\psi$, $J/\psi \to e^+e^-$ events. Dots with error bars are data and the histgram is Monte Carlo data. The distributions are smooth through the rib regions.

Muon Id

Here we only have one PID system to identify high energy muons so it is not possible to use the events themselves to determine the muon PID efficiency and background as in the electron case. Tracks are defined to be muons if they are found to have at least 2 good hits in the muon system as defined by the routine MYMUID [5]. Muon events can be defined requiring either 1 or 2 muon tracks. More events are obtained and better agreement between $B(ee)$ and $B(\mu\mu)$ is obtained if we allow both 2μ and 1μ track events. For 1μ events, an additional requirement $|(m_{\mu\mu} - m_{J/\psi})| < 0.25 GeV/c^2$ is made to reduce background. Fig. 8 shows the invariant mass distribution ($m_{\mu\mu}$) of the events with only one identified muon track. This distribution has been fit using the signal shape of the two muon track events plus a polynomial background. The background under the data within the cut region is small, about 5% of the 1 muon track events in the cut region or less than 1% of total sample of 1-μ and 2-μ track events. The 1-μ events make up about 14% of the $\mu\mu$ event sample.

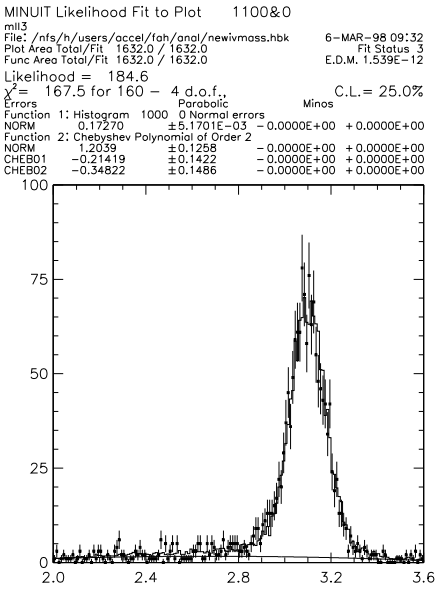

Figure 8: Invariant mass distribution ($m_{\mu\mu}$) of $\pi^+\pi^-\mu^+\mu^-$ events with only one muon track identified by the muon system. Data (points with error bars) are fit with signal (from events with both muons identified by the muon system and background (2nd order). Background in cut region between 2.85 and 3.35 GeV/c^2 is small.

Event Selection

Most $\psi' \to \pi^+\pi^- J/\psi$, $J/\psi \to l^+l^-$ events occur in the 4 prong sample, however a significant contribution is found in the > 4 prong sample. We will begin by describing the 4 prong selection.

Pion Cuts:

The pion cuts are the same as in the "Analysis Note on the Number of ψ''s" but are given again for convenience.

- good run (PPRUNS: status > 0 or 1).
- mnfit = 2, -9, -19.
- $|\cos\theta| < 0.75$ for π's
- $p_\pi < 0.5 GeV/c$
- $pxy(\pi) > 0.1 GeV/c$
- $\cos\theta_{\pi\pi} < 0.9$. $\theta_{\pi\pi}$ is the laboratory angle between the π^+ and π^-. This cut is used to eliminate contamination from misidentified e^+e^- pairs from γ conversions.
- $3.0 < m_{recoil} < 3.2 GeV/c^2$

These are the cuts used to select events for determining $B(J/\psi \to l^+l^-)$, where a fit is done to determine the number of $\psi' \to \pi^+\pi^- J/\psi$, $J/\psi \to l^+l^-$ events. However when selecting a sample for other purposes, like checking background in the ee events, additional cuts are made on the π's to reduce background:

- $\Sigma Hit_\pi^{dE/dx} > 13$. $\Sigma Hit_\pi^{dE/dx}$ is the number of hits used in the dE/dx calculation.
- $|\chi_\pi^{dE/dx}| < 3.0$. $\chi_\pi^{dE/dx} = \frac{(dE/dx)_{meas} - (dE/dx)_{exp}}{\sigma}$.

Initial Lepton Cuts

- Events must satisfy PID requirements described in the previous section.
- $0.5 < p_l < 2.5 GeV/c$
- $|\cos\theta| < 0.75$ for electrons, < 0.60 for muons.

With these cuts, there is still background in the electron sample. See Figs. 9 A-D. There are many more data events where both tracks have low momentum than there are for Monte Carlo events in the electron event samples. The muon events look much cleaner.

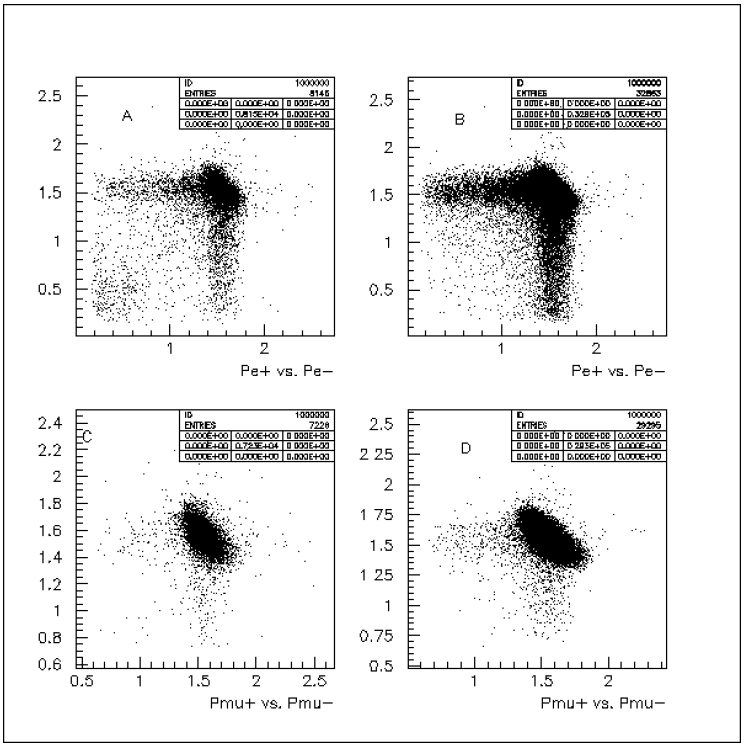

Figure 9: Plot of p_{l^+} versus p_{l^-} for $\psi' \rightarrow \pi^+\pi^- J/\psi$, $J/\psi \rightarrow l^+l^-$ events. A.) p_{e^+} vs p_{e^-} for $\pi^+\pi^- e^+e^-$ events. The cluster at low p is background. B.) p_{e^+} vs p_{e^-} for Monte Carlo $\pi^+\pi^- e^+e^-$ events. C.) p_{μ^+} vs p_{μ^-} for $\pi^+\pi^-\mu^+\mu^-$ events. D.) p_{μ^+} vs p_{μ^-} for Monte Carlo $\pi^+\pi^-\mu^+\mu^-$ events.

Additional Lepton Cuts

In order to reduce the background, we use additional kinematic cuts:

- $\cos\theta_{l^+l^-} < -0.85$. This is the cosine of the angle between the two leptons in the lab. See Fig. 10. The leptons from this decay are almost back to back.

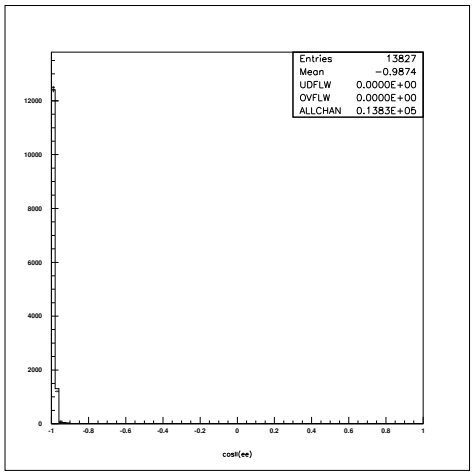

Figure 10: Cosine of the angle between the two leptons in $\pi^+\pi^-e^+e^-$ events ('95 data). Dots with error bars are data; histogram is Monte Carlo data.

- $\cos\theta^{cm}_{l^+l^-} < -0.975$. This is the cosine of the angle between the two leptons in the J/ψ CM. See Fig. 11. The leptons are even more back-to-back in the CM system.

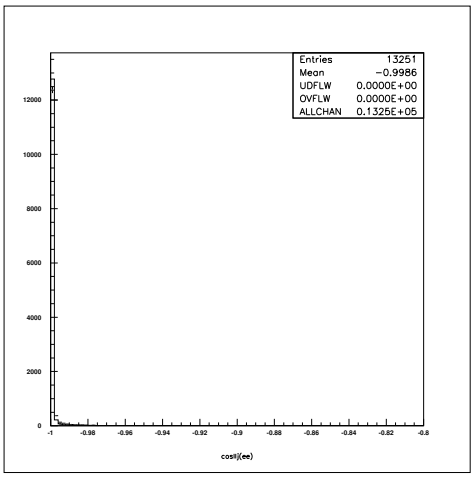

Figure 11: Cosine of the angle between the two leptons in $\pi^+\pi^-e^+e^-$ events ('95 data). Dots with error bars are data; histogram is Monte Carlo data.

- p_{l^+} or $p_{l^-} > 1.3GeV/c$ or $p_{l^+} + p_{l^-} > 2.4GeV/c$. This cut is used to cut out the background region (see Fig. 9A.)

Selection of > 4 Prong Events.

There is small but significant number of events in the > 4 prong sample. These events are primarily events where the hits on one low energy π track have been used to form two fitted tracks, which have nearly the same angles and momenta. Some of the track hits are used in one fitted track, and other hits are used in the other fitted track.

These events are potentially much more complicated than the 4 prong events, so in addition to the cuts mentioned above, the following cuts are made to simplify the analysis and to reduce background:

1. $2.2 > p_l > 1.0$ GeV/c.
2. $7 > NCHRG > 4$.
3. Only one good ee pair or $\mu\mu$ pair.

The m_{recoil} distribution for the > 4 prong events is shown in Fig. 12. Although the distribution has more background than the 4-prong events, there are clearly many signal events in the plot. The same fitting procedure is used to extract the signal as is used to extract the number of inclusive J/ψ events. The contribution of the > 4 prong events (fitted) is indicated in Table 3.

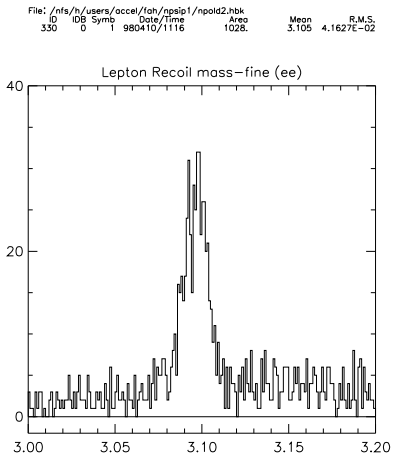

Figure 12: Number of events versus m_{recoil} for > 4 prong event sample. A clear signal is seen corresponding to the J/ψ peak.

Table 3: Contribution of > 4 prong events

Sample	$\mu\mu$ events (%)	ee events (%)
'93 data	4.0	3.6
'95 data	4.4	3.8

Hadronic Background Check.

It is important to test whether there are hadronic events getting into the $\psi' \to \pi^+\pi^- J/\psi, J/\psi \to l^+l^-$ events. To do this, we analyzed Daniela's $\rho\pi$ events from the '95 data.

Daniela's Cuts:

- ICODE > 0
- $1 < NNEU < 9$
- NCHRG $= 4$
- $\Sigma q_i = 0$
- $E_\gamma > 0.05$GeV
- $\cos\gamma < 0.96$
- $|\cos\theta| < 0.8$
- $\chi^2 < 20$ (4C fit)
- π^o mass cut: 50 MeV
- recoil mass against low momentum pair: (3.0 - 3.2 GeV/c^2)
- ρ cut: $0.6 < m(\pi\pi) < 0.95 GeV/c^2$

NOTE: Cuts to eliminate ee and $\mu\mu$ events were not used.

The events were analyzed thru the $\psi' \to \pi^+\pi^- J/\psi, J/\psi \to l^+l^-$ programs. The results are shown in Table 4.

Table 4: $N(\pi\pi\rho\pi)$ Results For '95 Data.

Cuts	Events
None	1350
π cuts and $\cos\theta_{l^+l^-}$ cut	471
Also Require lepton ID	21
Plus p_l cuts, and $\cos\theta^{cm}_{l^+l^-}$ cut	10

We can use these results to make a background estimate. Daniela obtains: $\epsilon(\pi\pi\rho\pi) = 0.12$. We assume $\epsilon(\pi^+\pi^-\pi^+\pi^-) \approx \epsilon(\pi\pi ll)$. Then

$$N_{BKG} = 10\frac{\epsilon(\pi\pi ll)}{\epsilon(\pi\pi\rho\pi)} = 24$$

$$\%BKG = 24/27000 = 0.1\%$$

The amount of background due to $\psi' \to \pi^+\pi^- J/\psi, J/\psi \to \rho\pi$ events is negligible. In fact, the estimate is probably an overestimate, since potential $J/\psi \to l^+l^-$ events that Daniela vetoed were kept in the sample. This channel should be one of the largest contributors to hadronic background. There are many other channels, but most of them have either higher multiplicities or higher mass particles and will be killed even more effectively by our kinematic cuts. Therefore the hadronic background is expected to be small.

Monte Carlo

The Monte Carlo generator used is PPGEN. A total of 200,000 (153 realization) plus 370,000 (154 realization) Monte Carlo events are generated each for the $\psi' \to \pi^+\pi^- J/\psi$, $J/\psi \to e^+e^-$ and $\psi' \to \pi^+\pi^- J/\psi$, $J/\psi \to \mu^+\mu^-$ samples.

The Monte Carlo[6] assumes:

1. The orbital angular momentum between $\pi\pi$ system and J/ψ and between π's in the $\pi^+\pi^-$ system is 0.

2. The mass of the $\pi\pi$ system is weighted towards high mass.

$$\frac{d\sigma}{dm_{\pi\pi}} \propto \text{phase space} \times (M^2_{\pi\pi} - 4m^2_\pi)^2$$

3. Sequential 2-body decays: $\psi' \to X + J/\psi$, $X \to \pi^+\pi^-$, and $J/\psi \to l^+l^-$.

4. X and J/ψ are uniformly distributed in $\cos\theta$.

5. π's are uniformly distributed in $\cos\theta_\pi$ in the X rest frame.

6. Leptons have $1 + \cos^2\theta$ distribution in J/ψ rest frame.

7. J/ψ decay has α^3 order final state radiative correction in CMS of J/ψ.

Data - Monte Carlo Comparison.

Figs. 13-16 show a comparison of data and Monte Carlo for an assortment of plots. The agreement is good, in general, confirming that the cuts used eliminate background. However, the Monte Carlo does not fit the m_{recoil} distribution well.

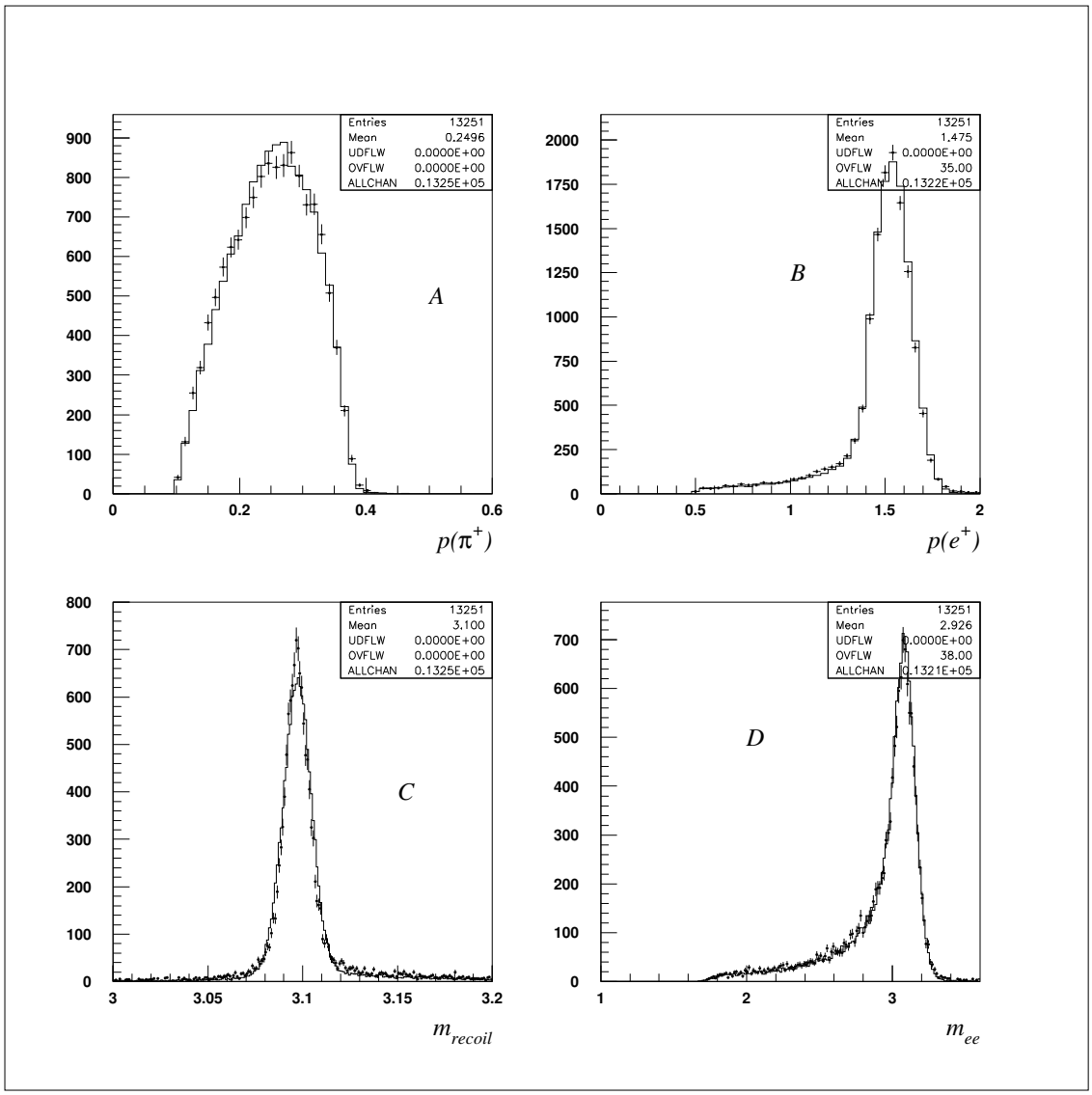

Figure 13: Comparison between $\psi' \to \pi^+\pi^- J/\psi$, $J/\psi \to e^+e^-$ data (dots with error bars) and Monte Carlo data (histogram). A.) p_{π^+}. B.) p_{e^+}. C.) m_{recoil}. D.) $m_{e^+e^-}$.

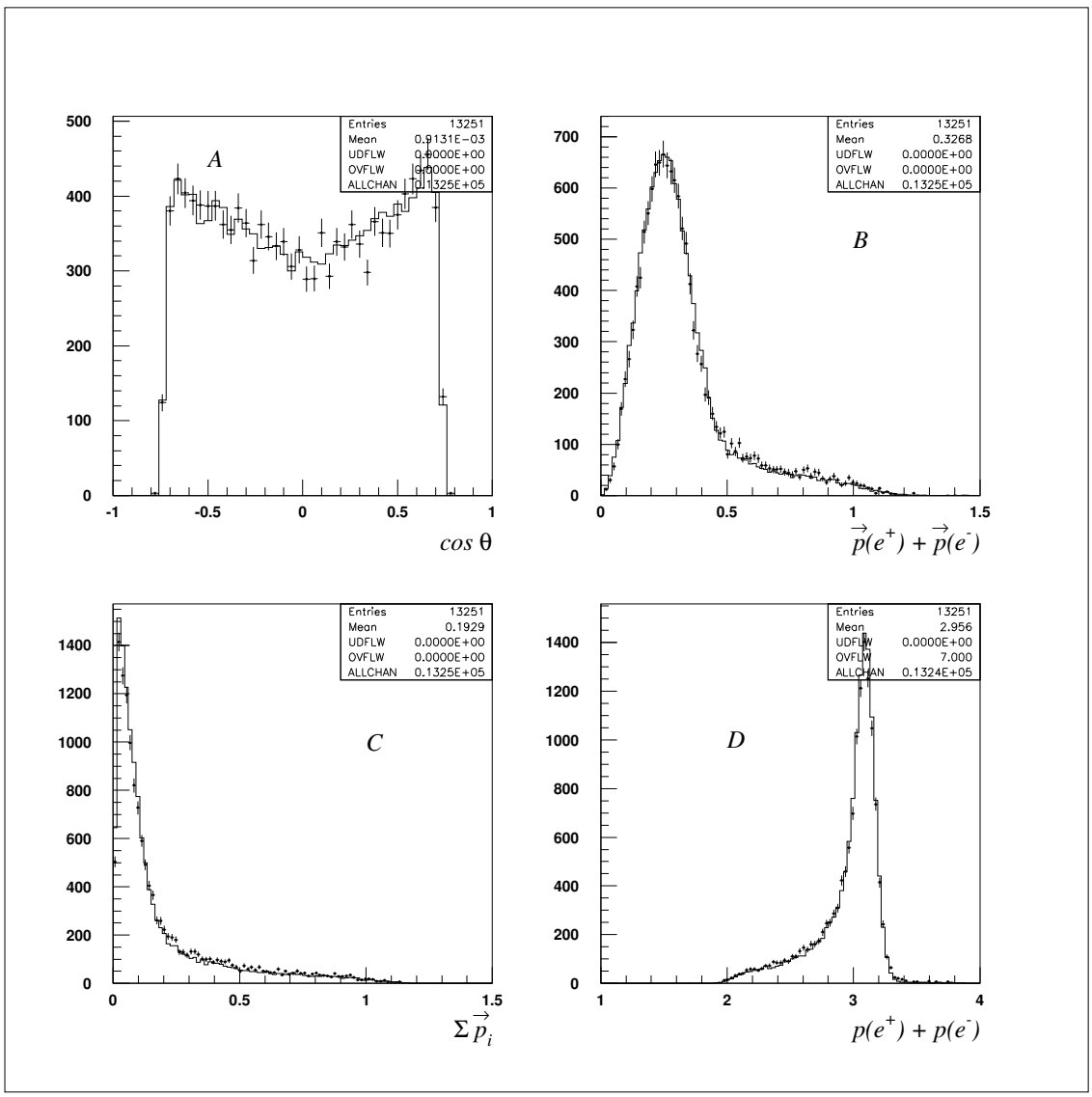

Figure 14: Comparison between $\psi' \to \pi^+\pi^- J/\psi$, $J/\psi \to e^+e^-$ data (dots with error bars) and Monte Carlo data (histogram). A.) $\cos\theta_e$ distribution. B.) $\vec{p}(e^+) + \vec{p}(e^-)$ distribution. C.) $\Sigma_{i=1}^{4}\vec{p}_i$ distribution. D.) $p(e^+) + p(e^-)$ distribution.

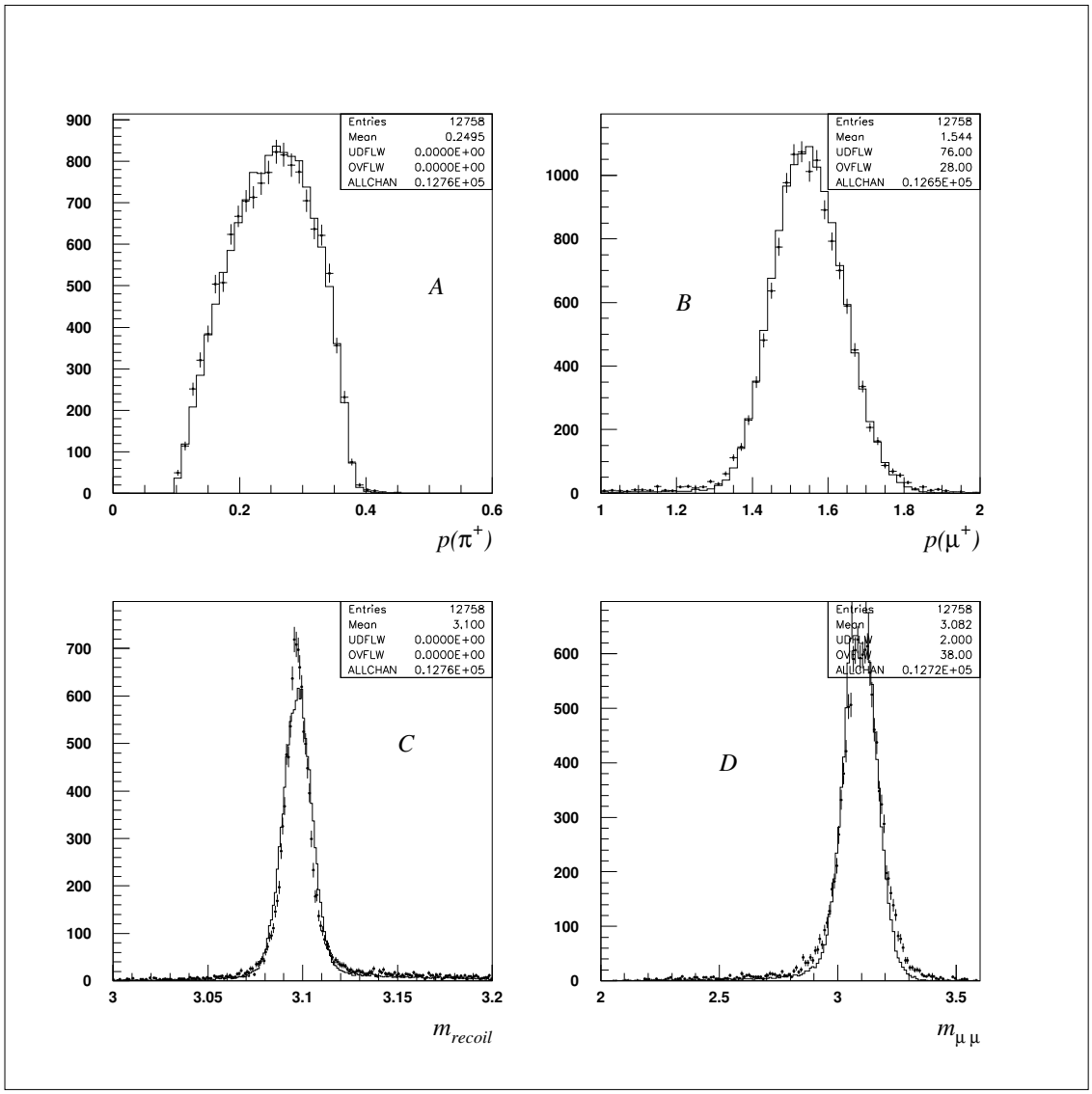

Figure 15: Comparison between $\psi^{'} \to \pi^+\pi^- J/\psi$, $J/\psi \to \mu^+\mu^-$ data (dots with error bars) and Monte Carlo data (histogram). A.) p_{π^+} B.) p_{μ^+} C.) m_{recoil} D.) $m_{\mu^+\mu^-}$

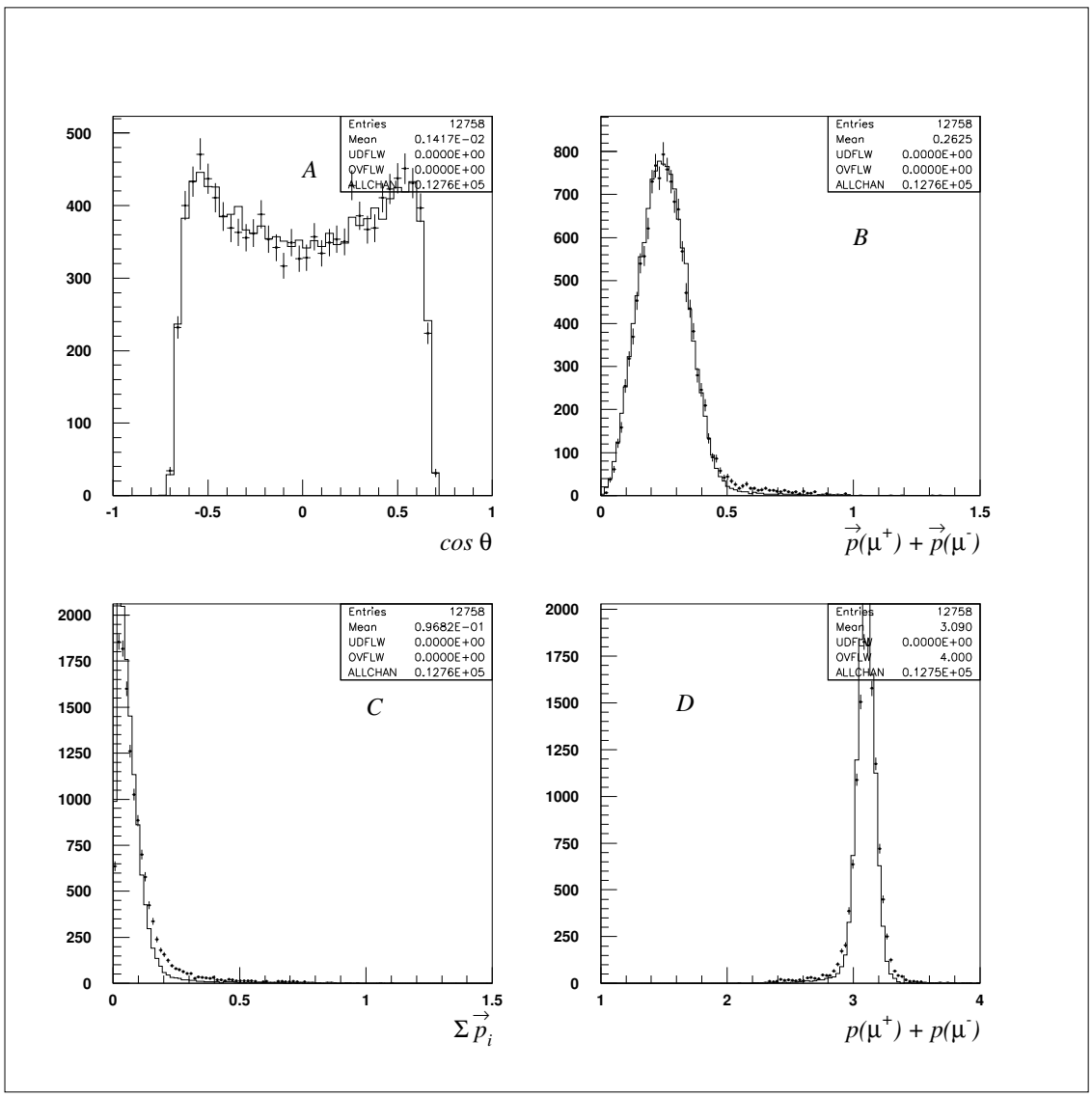

Figure 16: Comparison between $\psi' \to \pi^+\pi^- J/\psi$, $J/\psi \to \mu^+\mu^-$ data (dots with error bars) and Monte Carlo data (histogram). A.) $\cos\theta_\mu$ distribution. B.) $\vec{p}(\mu^+) + \vec{p}(\mu^-)$ distribution. C.) $\Sigma_{i=1}^{4}\vec{p}_i$ distribution. D.) $p(\mu^+) + p(\mu^-)$ distribution.

Fitting

For the $\pi\pi ll$ events satisfying cuts, the mass recoiling against the π's, m_{recoil}, is calculated, and the m_{recoil} distribution is fitted using BWFIT to determine the number of $\pi\pi ee$ and $\pi\pi\mu\mu$ events, just as was done to determine the amount of J/ψ signal, as described in Ref. [1]. The fit uses a Breit Wigner smeared by a Gaussian (BWG) for the signal plus a 3rd order polynomial to describe the "background". The BWG parameters used in this fit are obtained from the m_{recoil} distribution for $\psi' \to \pi^+\pi^- J/\psi$ events, where $J/\psi \to l^+l^-$. Most of the events associated with the polynomial are good $\psi' \to \pi^+\pi^- J/\psi$ events but where the low energy π's undergo $\pi \to \mu\nu$ decay. Using only the BWG curve to describe the signal shape makes us less sensitive to background. The fitting is done separately for '93 and '95 data.

Branching Ratio Results

The results are given in Table 5. NOTE: The small corrections for backgrounds and for data-Monte Carlo efficiency differences for leptons have not been put in. These differences will be included in the systematic errors.

Table 5: RESULTS. Status > 1.

Result	'93 Data	'95 Data
$N_{\mu\mu}$ (Fitted)	5201	9410
N_{ee} (Fitted)	6389	11730
$N\psi'$	1.29×10^6	2.37×10^6
$B(ee)$	$(5.876 \pm 0.085)\%$	$(5.917 \pm 0.063)\%$
$B(\mu\mu)$	$(5.913 \pm 0.094)\%$	$(5.799 \pm 0.068)\%$

Study of Systematic Errors

The effect of changing the π cuts has been studied. The results are shown in Table 6. There are other potential contributions to the systematic error. The Monte Carlo program assumes that the cosine of the π^+ angle, $\cos\theta_{\pi^+}$, in the $\pi\pi$ center of mass system is flat (S wave). However, as is predicted in one Heavy Quarkonium Model [7], we find that this distribution is not flat, consistent with a small amount of D-wave. If we assume a $\cos\theta_{\pi^+}$ distribution, consistent with our data, we obtain slightly different results, as indicated in Table 6.

Another possible systematic error is due to our fitting procedure, where we fit the $N_{J/\psi}$ "signal" to a BWG. An alternative procedure using MINFIT[3] has also been used in Hawaii. In this method, the inclusive m_{recoil} is fit directly with the exclusive m_{recoil} distribution (histogram), so there is no forcing the data to fit an arbitrary shape. The difference between the BWG fit and the MINFIT fit is also given in Table 6 and is small.

As mentioned previously, similar calculations have been done at Hawaii and IHEP. The methods share a great deal in common but are not completely identical. However there is good agreement between the two calculations. For status > 1, Meng obtains $B(J/\psi \to ee) = 5.84 \pm 0.08$ and $B(J/\psi \to \mu\mu) = 5.82 \pm 0.09$ for the '93 data and $B(J/\psi \to ee) = 5.87 \pm 0.06$ and $B(J/\psi \to \mu\mu) = 5.75 \pm 0.07$ for the '95 data. For more detail, see Ref. [8].

Another contribution comes from the efficiency determination. As described in Ref. [1], the efficiency $\epsilon_{J/\psi}$ depends on the produced multiplicity distribution given by ω_k. Using the systematic error in $\Delta\epsilon_{J/\psi}$, as well as statistical uncertainties in the efficiencies determined by the Monte Carlo programs yields the results shown in Table 6.

Adding the systematic errors, except for Run Status, in quadrature, we obtain the systematic errors given in Tables 6 and 7.

Table 6: Branching Ratio Systematic Errors (%)

Variable	Change	'93 $B(ee)$	'93$B(\mu\mu)$	'95 $B(ee)$	'95$B(\mu\mu)$
Run Status	$> 1 \to > 0$	0.43	0.05	0.12	0.84
$\lvert\cos\theta_\pi\rvert$ cut	$0.75 \to 0.70$	0.60	0.88	0.00	0.66
$\cos\theta_{\pi\pi}$ cut	$0.9 \to 0.85$	0.05	0.00	0.08	0.10
p_{xy} cut	turn off	0.60	0.61	0.39	0.53
$\lvert\cos\theta_\mu\rvert$ cut	$0.6 \to 0.65$	0.15	0.66	0.00	0.00
$\lvert\cos\theta_e\rvert$ cut	$0.75 \to 0.7$	0.24	0.07	0.42	0.12
$\cos\theta_{l^+l^-}$ and $\cos\theta^{cm}_{l^+l^-}$ cuts	turn off	0.56	0.32	0.41	0.26
E/p cut	$0.6/p \to 0.7/p$	0.18		0.19	
p_l^+ or p_l^-	$> 1.3 \to > 1.4$ GeV/c	0.31	0.03	0.30	0.03
p_l^+ and p_l^-	$> 0.5 \to > 0.8$ GeV/c	1.01	0.07	0.82	0.10
Non-flat $\cos\theta_\pi$		0.03	0.02	0.02	0.02
mfit = 2		0.53	1.12	0.07	0.05
Fitting Method		0.33	1.14	0.50	0.17
Efficiency Uncertainty		0.49	0.53	0.37	0.41
PID Uncertainties		0.90	0.10	0.80	0.20
Hawaii/IHEP Difference		0.61	1.57	0.79	0.84
Combined		2.04	2.67	1.74	1.36

Final Results

Using the results from Table 6 to determine the systematic errors, we obtain the results shown in Table 7.

Table 7: FINAL RESULTS. Status > 1

Result	'93 Data (%)	'95 Data (%)
$B(ee)$	$5.876 \pm 0.085 \pm 0.120$	$5.917 \pm 0.063 \pm 0.103$
$B(\mu\mu)$	$5.913 \pm 0.094 \pm 0.158$	$5.799 \pm 0.068 \pm 0.079$

Combining:

$$B(ee) = (5.903 \pm 0.051 \pm 0.103)\%$$

$$B(\mu\mu) = (5.838 \pm 0.055 \pm 0.099)\%$$

The close equality of B_μ and B_e is a verification of e-μ universality:

$$\frac{B(J/\psi \to e^+e^-)}{B(J/\psi \to \mu^+\mu^-)} = 1.011 \pm 0.013 \pm 0.016.$$

Assuming $B_\mu = B_e$, we find a combined leptonic branching fraction of

$$B(ll) = (5.867 \pm 0.037 \pm 0.090)\%$$

The four values in Table 7 are in reasonable agreement; when compared to $B(ll)$, they give a $\chi^2 = 1.92$ using only the statistical errors, corresponding to a $CL \approx 60\%$.

Our results are compared with previous experiments in Table 8. These results are consistent with and improve on the precision of the MARK-III measurement [10]. They are also consistent with BES results determined from e^+e^- cross section measurements in the vicinity of J/ψ resonance [11]. If we combine the values of $B(ll)$, we obtain a new world average

$$B(ll) = (5.894 \pm 0.086)\%,$$

which has an error about half that in the 1996 PDG[12].

Table 8: Comparison with other experiments

Experiment	$B(ee)(\%)$	$B(\mu\mu)(\%)$
Mark I [9]	6.9 ± 0.9	6.9 ± 0.9
Mark III [10]	$5.92 \pm 0.15 \pm 0.20$	$5.90 \pm 0.15 \pm 0.19$
BES Scan [11]	6.09 ± 0.33	6.08 ± 0.33
THIS EXPERIMENT	$5.903 \pm 0.051 \pm 0.103$	$5.838 \pm 0.055 \pm 0.099$

The experimental ratio of the quarkonium annihilation rates

$$R_2 = \frac{\Gamma(quarkonium \to ggg)}{\Gamma(quarkonium \to \mu^+\mu^-)}$$

allows the determination of the strong coupling constant α_s or, equivalently, the QCD scale parameter $\Lambda_{\overline{MS}}^{(n_f)}$ [13, 14]. Following the notation of ref. [14], one obtains

$$\begin{aligned}(1+R_1)R_2 &= [1 - 2B(J/\psi \to l^+l^-) \\ &- B(J/\psi \to \gamma^* \to q\bar{q}) \\ &- B(J/\psi \to \gamma\eta_c)]/B(J/\psi \to l^+l^-)\end{aligned}$$

where,

$$R_1 = \frac{\Gamma(J/\psi \to \gamma gg)}{\Gamma(J/\psi \to ggg)} = \frac{16\alpha}{5\alpha_s}(1 - 3.0\frac{\alpha_s}{\pi}),$$

$$R_2 = \frac{\Gamma(J/\psi \to ggg)}{\Gamma(J/\psi \to l^+l^-)} = \frac{5(\pi^2-9)\alpha_s^3}{18\pi\alpha^2}(1 + 1.59\frac{\alpha_s}{\pi})\gamma_\psi,$$

and

$$\gamma_\psi = \frac{\Gamma(c\bar{c} \to ggg)}{\Gamma^0(c\bar{c} \to ggg)} = 0.31 \pm 0.03.$$

The factor γ_ψ is the reduction factor of the three gluon decay caused by the finite size effect in the matrix element. For R_1, we use the theoretically calculated rather than the measured value because of the large error associated with the latter [15].

Combining the above J/ψ decay parameters and the values for $B(J/\psi \to \gamma^* \to q\bar{q})$, $B(J/\psi \to \gamma\eta_c)$ listed in PDG[12], we obtain

$$\alpha_s(m_c = 1.5GeV/c^2) = 0.28 \pm 0.01 \quad \text{and}$$

$$\Lambda_{\overline{MS}}^{(4)} = (209 \pm 21)MeV,$$

where only the experimental errors are included. Our results are in good agreement with the PDG[12] values.

References

[1] See: "Analysis Note: Number of ψ' Events", F. A. Harris and Wang Meng, March 98.

[2] Bill Dunwoodie and Li Xinhua have studied the dE/dx TOF information for the ψ' data and have written routines to correct it.

[3] MnFit: Brock, I. C., L3 Note 918, June 1994. Here we shift and scale the Monte Carlo E/p distribution using:

$$(E/p)_{new} = scale * (E/p)_{old} + shift.$$

[4] OKSPI was written by Yuan Changzheng. It corrects for the observed mean shift and then uses 3 σ cuts in terms of the measured σ for each data set.

[5] MYMUID was written by Yuan Changzheng. It checks the track matches in the muon counters after making empirical shifts to the counters positions. My version corrects a mistake in this routine. I have also checked that I obtain the same results not using this routine and just using the muon bits directly.

[6] BES Collaboration, "Determination of the J/ψ Leptonic Branching Fraction via $\psi(2S) \to \pi^+\pi^- J/\psi$", draft of Oct. 94.

[7] V. A. Novikov and M.A. Shifman, Z. Phys. 8, 43 (1981).

[8] Wang, Meng, "The Total Number of Psi' Events", Nov. 1996;
Wang, Meng, "Precious Measurement of Branching Ratios for $J/\psi \to l^+l^-$ and Determination of Total Number of psi' at BES", June 1997.

[9] A. M. Boyarski et al., Phys. Rev. Lett. 34, 1357 (1975).

[10] D. Coffman et al., Phys. Rev. Lett. 68, 282 (1992).

[11] J. Z. Bai et al., Phys. Lett. B 355, 374 (1995).

[12] PDG

[13] W. Kwong et al., Phys.Rev. **D37** (1988) 3210.

[14] H.C. Chiang et al., Phys.Lett. **B324** (1994) 482.

[15] D.L. Scharre et al., Phys.Rev. **D23** (1981) 43.